# PCCP

## Accepted Manuscript

This is an *Accepted Manuscript*, which has been through the Royal Society of Chemistry peer review process and has been accepted for publication.

*Accepted Manuscripts* are published online shortly after acceptance, before technical editing, formatting and proof reading. Using this free service, authors can make their results available to the community, in citable form, before we publish the edited article. We will replace this *Accepted Manuscript* with the edited and formatted *Advance Article* as soon as it is available.

You can find more information about *Accepted Manuscripts* in the **Information for Authors**.

Please note that technical editing may introduce minor changes to the text and/or graphics, which may alter content. The journal's standard **Terms & Conditions** and the **Ethical guidelines** still apply. In no event shall the Royal Society of Chemistry be held responsible for any errors or omissions in this *Accepted Manuscript* or any consequences arising from the use of any information it contains.

# ARTICLE TYPE

# Controlled growth of large area multilayer graphene on copper by chemical vapour deposition

**Sibel Kasap,[b] Hadi Khaksaran,[a,b] Süleyman Çelik,[b] Hasan Özkaya,[b] Cenk Yanık,[a,b] and Ismet I. Kaya,[a,b]**

The growth of nearly full coverage of multilayer graphene on the surface of a 99.8% purity copper foil has been experimentally studied. It has been shown that the film thickness can be controlled by a single parameter, the growth time, and growth can be extended until nearly full coverage of more than one layer
10 graphene over the copper surface. The results are supported by scanning electron microscopy and Raman analysis together with optical transmittance and sheet resistance measurements. It has been verified that silicon oxide impurity particles within the copper act as catalysts and the seeds of multilayer graphene islands. The linear increase of the average thickness of graphene to the growth time have been attributed to the interplay between the mean distance between the impurities on the surface and molecular mean free
15 path in the process gas. A qualitative model is proposed to explain the microscopic mechanism of the multilayer growth on copper. These results contribute understanding of the chemical vapour deposition growth kinetics towards the objective of large area high quality graphene production with tuneable layer thickness.

## Introduction

20 Graphene is a unique material, which has drawn significant attention because of its extremely high carrier mobility, tuneable band gap and high elasticity.[1–4] Therefore, it is considered as to have a great potential to be utilized in a range of electronic devices including solar cells, field effect transistors, super-
25 capacitors, batteries, displays and sensors. [4–11]A significant amount of research has been devoted for the synthesis of graphene since its large scale production with controllable parameters will be a key factor towards commercialization. Exfoliating graphene from graphite either mechanically[12] or
30 chemically[13]creates small flakes, that are not suitable for applications requiring uniformity. High quality graphene can be synthesized epitaxially on the surface of a SiC substrate by desorption of Si atoms.[14] However, SiC epitaxy has intrinsic limitations for large area applications. Yet another method to
35 produce graphene is to synthesize it on a metal catalyst substrate by chemical vapour deposition (CVD).[15–23] Currently, CVD appears to have the greatest potential for large area production of graphene with sufficiently high crystalline quality for optoelectronic applications.
40 The potential of graphene in optoelectronics lies in the fact that it can have both high transparency and high conductivity at the same time. With its enormous flexibility, graphene is one of the outstanding candidate materials as a transparent conductive electrode for flexible electronics. Nearly 98% transparency of
45 single layer graphene is far superior to those required by the most of the optoelectronic applications. However obtaining a high conductivity graphene with high stability is proven to be a challenge. Although single crystal graphene can have very high mobility as demonstrated in small mechanically exfoliated
50 samples, larger sheets synthesized by scalable methods such as CVD show much lower mobility values. Besides, it is difficult to control the unintentional doping of such a one atom thick material. The sheet resistance of monolayer CVD grown graphene typically ranges from several hundreds to a thousand
55 Ohms per square.[24–26] The reduced conductance in CVD graphene is due to crystal domains and defects inherently formed during its growth. Therefore, it seems to be a more viable approach to use multilayer graphene to achieve a better conductivity with a slightly reduced transparency within the
60 acceptable limits. In that sense, multilayer graphene appears to be closer to meet the current $10\text{-}500\Omega/\square$ and 80-90%transparency requirements for a variety of applications such as displays or touch screens.[27–30]

Copper and nickel are the most widely used transition metals
65 for the metal-assisted CVD synthesis of graphene.[31–34] Material parameters, such as carbon solubility, crystal structure and lattice constant as well as the thermodynamic parameters affect the deposition of graphene on the surface of a catalyst metal.[15,35,36] Low carbon solubility in copper predominantly limits the growth
70 of graphene to single-layer films and the growth is mainly due to the surface adsorption of carbon atoms.[31,37] However, recently it has been demonstrated that multilayer graphene films can also be grown on copper under certain CVD conditions.[9,24,38–45]Aside

from the CVD conditions, qualities of the copper foil such as surface roughness, crystal domain size and orientation, density of defects and impurities appear to play a role in the formation of multilayer graphene.[24,25,41,46] Previous studies revealed that the presence of impurities increases the activity of a catalyst at its surface by enhancing the surface reaction rate. Therefore, the graphene thickness was locally increased in the vicinity of the impurities or surface defects due to the increased amount of dissociated carbon atoms.[24,47,48] However, growing uniform multilayer graphene on copper with a predetermined thickness and coverage still stands as an open problem as number of layers of graphene and their coverage was not changing much after initial few minutes of growth time.[48–50] On the other hand, though using nickel or nickel-copper alloy, instead of copper can provide full coverage multilayer graphene, but with conductivity that still does not meet the requirements for most of the electro-optical applications.[51–54]

In this work, we investigated formation multilayer graphene islands on the surface of a copper foil by varying the growth time during the CVD process until reaching almost full coverage. The results confirm that in the presence of nano particle impurities, both the average thickness and the surface coverage of graphene increase with the growth time. The results suggest the role of the process pressure and the density of the impurities on the multilayer graphene growth kinetics.

## Experimental methods

### Graphene growth and transfer

A chemical vapour deposition setup with a 120 mm diameter quartz tube was used to synthesize graphene. A copper foil with 25 μm thickness and 99.8% purity purchased from Taiwan Copper Foil Co. was used as the catalytic metal substrate. The foil is wrapped around a 10 cm (outer diameter) x 50 cm (length) quartz tube, which is centered in the outer tube. This configuration allows the growth of graphene on copper substrates with up to 30 cm diagonal size. The CVD process was started by annealing the copper foil at 1000 °C for 20 minutes under 200 sccm flow of $H_2$ to treat the surface. This was followed by the growth phase (1-25 minutes) during which a mixture of 50 sccm $CH_4$ and 200 sccm $H_2$ was delivered at 1000 °C temperature and 60 mbar process pressure. The chamber pressure was attained by a dry pump at the exhaust and measured by using a high accuracy mechanical gauge. Finally, the chamber was cooled down with 200 sccm of argon flow until it reached the room temperature. Cooling of the chamber from 1000 °C to 200 °C takes 10 minutes.

After the growth, a wet transfer process is used to transfer graphene films from the copper to $SiO_2$/Si and glass substrates for electrical, optical and Raman characterization. In order to support the graphene film, a thin layer of PMMA (MicroChem 950 PMMA 2% in chlorobenzene) was spin-coated at 4000 rpm for 45 s on the as-grown samples and baked at 180°C for 5 minutes. With the purpose of improving the efficiency of the wet chemical etching, inadvertently grown graphene at the back-side was removed by oxygen plasma. Then the samples were placed in a 0.1 M aqueous $(NH_4)_2S_2O_8$, for about 15 hours. After the copper foil was completely etched away, the graphene film with PMMA coating was transferred from the solution into DI water. Three cycles of 10 minutes DI water rinsing were applied to completely wash away the remaining etchants. Then a pre-cleaned $SiO_2$/Si or a glass substrate was dipped into water and the film was picked up. Finally the PMMA was dissolved using a hot acetone bath at 70 °C, rinsed with 2-propanol and dried in air.

### Characterization

To structurally characterize the graphene and copper samples, scanning electron microscopy (SEM, Zeiss Gemini 1530), energy dispersive spectroscopy (EDS, OXFORD INSTRUMENTS X-Max[N]), inductively coupled plasma optical emission spectrometry (ICP-OES, Perkin-Elmer 2000 DV), optical microscopy, and Raman spectroscopy (Renishaw in Via Reflex) were used. Raman spectroscopy and mapping were used to confirm the presence and uniformity of grown samples. The wavelength and the spot size of the Raman excitation laser was 532 nm and 2 μm respectively. The optical transmittance (T) and the conductivity measurements were performed on 1x1 cm2 graphene films transferred onto glass slides. The transmittance of the graphene was measured using a spectrophotometer (Bruker Equinox 55IR), where a bare glass slide was used as the reference. The sheet resistance ($R_s$) of the graphene samples was measured by Van der Pauw method.

## Results and Analysis

The coverage and the distribution of the graphene films were analysed by Raman, SEM and optical microscopy before and after the transfer. Multilayer graphene formation over a full coverage single layer graphene is seen in all of the samples (5, 10, 15, 20 and 25 minute growth time). We observed that the average thickness and the coverage of the multilayer graphene film show a steady increase as the growth time is increased.

Fig.1 illustrates the SEM images of the copper surfaces after CVD deposition. The adjacent pictures in the same figure are the optical microscopy images of the graphene from the same batches but after they were transferred on 300 nm $SiO_2$/Si substrates. In the SEM images, apart from the 20-50 μm size polygonal patches due to copper domains with distinct grey levels, there appear smaller scale dark regions spreading all over the surface. These dark regions correspond to bilayer and multilayer graphene islands formed over the nearly full coverage single layer graphene.
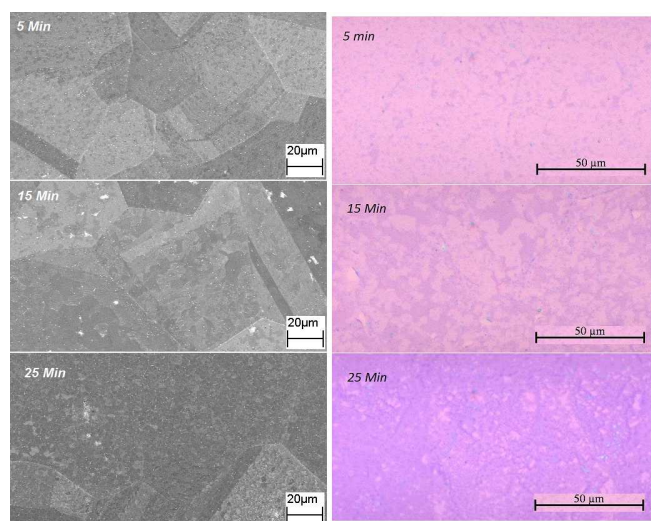
In the optical microscopy images of the transferred films, the dark purple regions correspond to multilayer graphene as verified by the Raman analysis. Both SEM and optical microscopy images reveal that while the surface is covered mostly with monolayer graphene for the 5 minute grown sample, multilayer coverage increases and spreads to all surface area as the growth time is increased.

In Fig. 2 the SEM images of multilayer graphene flakes with 5 and 25 minute growth times are compared at higher magnifications. There appear some impurity particles as bright white spots, typically located in the centre of the multilayer graphene flakes. The EDS analysis revealed that these nano particles that emerged at the surface of the copper foil are silicon oxide (Fig. 2 bottom). It has been verified in several studies that silicon oxide nano particles can act as catalysts for the growth of

# Journal Name

**Physical Chemistry Chemical Physics**

Dynamic Article Links ▶

## ARTICLE TYPE



**Fig. 1** SEM images of graphene films on Cu foil (left) and optical microscope images of transferred graphene on 300 nm SiO$_2$ (right). Labels 5 min, 15 min, 25 min indicate the growth time of the CVD
5 process.

graphene and carbon nano tubes.[55–58] They can effectively decompose hydrocarbons and become the nucleation centres during the formation of the first graphene layer and then the active carbon source for the growth of the successive layers.
10 Therefore, the presence of silicon oxide nano particles delivers a condition for an efficient growth of multilayer graphene.[24,25] To clarify the origin of SiOx impurities we carried out inductively coupled plasma optical emission spectrometry (ICP-OES) analysis on the etched solution of copper foil. The result of the
15 trace element analysis revealed that Si composed 94% of all the impurities. The analysis results for untreated and 20 minute annealed copper foil pieces yielded the same results confirming that the Si nanoparticles on the surface emerged from the copper foil. To determine the surface density of these nucleation centres
20 a very short growth time is applied on one sample. 1 minute growth formed patches of monolayer graphene each containing one nucleation centre in the middle. High contrast of graphene on copper as seen in the SEM image in Fig. 2 allowed accurate counting of graphene islands. The average nucleation density was
25 found to be n = 0.028/$\mu$m$^2$ and from that the mean distance between nucleation centres was calculated as $d$ = 6 $\mu$m.

Fig. 3a compares the Raman spectra of all the graphene films that were synthesized in 5 different growth durations and transferred on 300 nm SiO$_2$/Si substrates. All traces indicate high
30 quality graphene formation with distinct G and 2D peaks and small D peaks. Evolution of the 2D peak from the top to the bottom trace indicates thickening of graphene with the growth time; it broadens and its relative height to the G peak decreases. Shifting of 2D peak position towards lower energies also verify
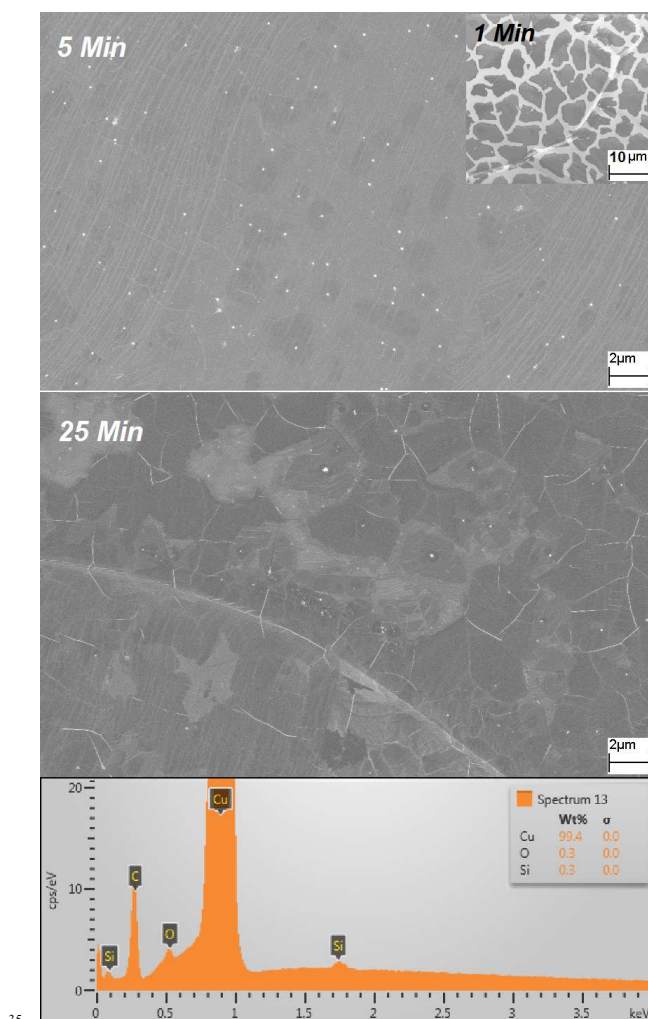


**Fig. 2** High magnification SEM images of graphene films on copper. 5 min. growth (top): Bilayer graphene patches are seen as separated light grey areas spread over single layer graphene that covers the surface. 25 min growth (middle): Bilayer and multilayer zones dominate over the
40 surface appearing as numerous levels of grey that cascades concentrically. In both images impurity particles are located centrally inside the bilayer/multilayer islands acting as their sources. 1 min. growth (top right): Graphene domains at earlier stages of growth provide accurate determination of the nucleation density. The EDS analysis of
45 bright white spots in the SEM images reveals they are SiOx (bottom).

increasing number of layers. A modal analysis of the 2D peak is performed to validate this conclusion. Fig. 3b and c exhibit the deconvolution analyses of the 2D peak for the samples with 5 and 15 minutes growth time. The 2D peak from graphene synthesized
50 for 5 minutes growth time has a single component. This symmetric and sharp 2D peak with FWHM of 28 cm$^{-1}$ confirms predominantly monolayer graphene on the surface.[59,60] On the other hand, the 2D peak of graphene synthesized for 15 minutes duration is composed of two Lorentzian curves 2D$_1$ and 2D$_2$

*Physical Chemistry Chemical Physics Accepted Manuscript*

# ARTICLE TYPE
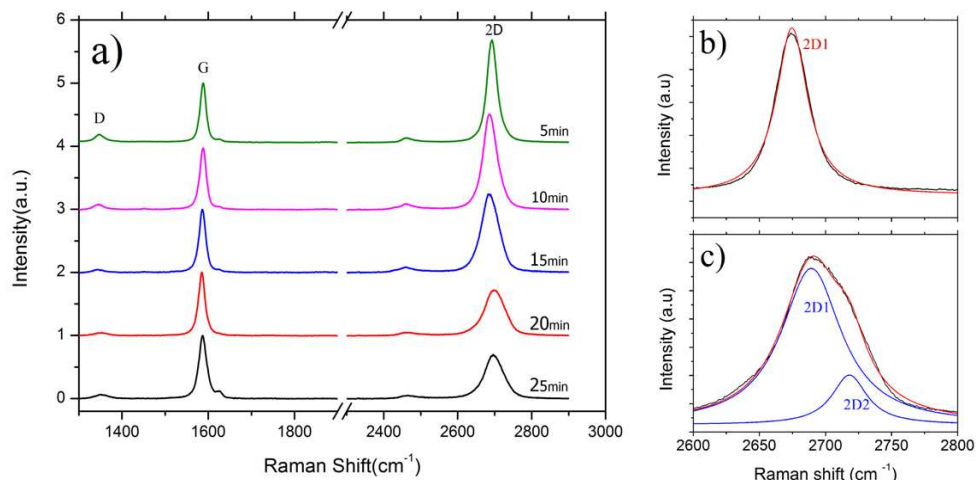


**Fig. 3** (a) Raman spectra from the graphene films transferred on 300 nm SiO₂. Each trace is obtained by averaging the data from five random points on a film and scaled to the same G peak height for better comparison. Labels denote the growth time. (b) and (c) show the measured Raman spectra and calculated 2D peak deconvolution for 5 min and 15 min samples respectively.
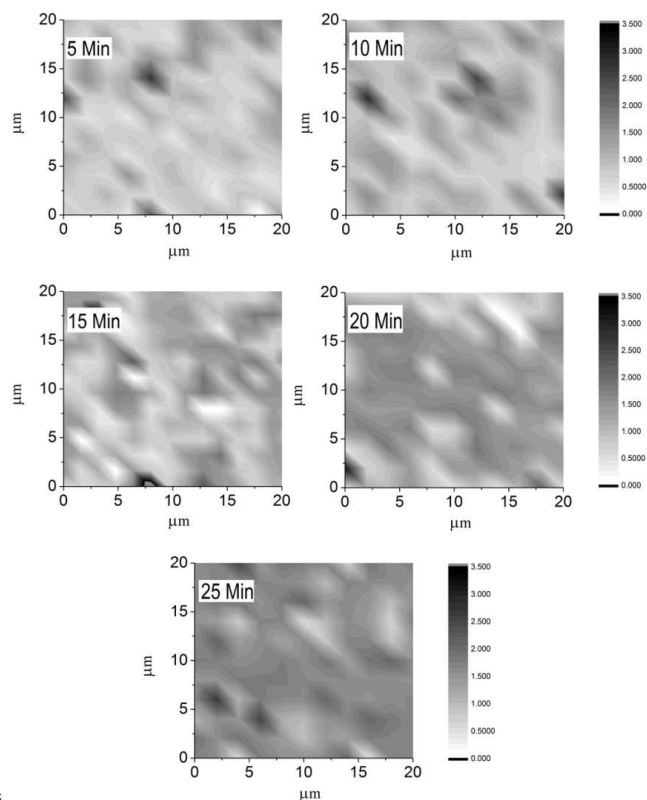


**Fig. 4** Raman mapping of transferred graphene films on 300 nm SiO₂. The colour scales represent the ratio of the intensities at the peaks, $I_G/I_{2D}$ and have the same range for all of the maps. Labels denote the growth time.

Table 1 Representative value of the average graphene thickness ($<I_G/I_{2D}>$) and bilayer-multilayer graphene surface coverage ($c_m$) for the samples with different growth times.

| Growth time (min.) | 5 | 10 | 15 | 20 | 25 |
|---|---|---|---|---|---|
| $<I_G/I_{2D}>$ | 0.80 | 1.04 | 1.12 | 1.20 | 1.56 |
| $c_m$ | 0.24 | 0.40 | 0.58 | 0.65 | 0.90 |

validating multilayer graphene formation.[61]

In order to determine the spatial distribution of multilayer graphene formation, a comprehensive Raman mapping is performed on the transferred films by taking the Raman spectrum of all the points on a 20x20 grid with 1 μm period. The Raman maps in Fig. 4 show the ratio of the G to 2D peak intensities ($I_G/I_{2D}$). $I_G/I_{2D}$ is an indicative measure of the thickness of graphene films, which is particularly useful for mapping.[48,59,61] The maps in Fig. 4 signify the positive correlation between the growth time and the graphene thickness.

A numerical analysis on these data was performed and the average values of $I_G/I_{2D}$ ratio over the surface of each sample were calculated (Table 1). Additionally, adopting the general convention of $I_G/I_{2D} \geq 1$ for bilayer and multilayer graphene films, surface coverage of bilayer and multilayer graphene ($c_m$) for each sample were also calculated and given in Table 1. Here $c_m$ is calculated as the fraction of the number of points with $I_G/I_{2D} > 1$ in the Raman map. These data show that both $<I_G/I_{2D}>$ and $c_m$ monotonously increase with increasing growth time. For 25 minutes growth time multilayer graphene on the surface spreads to 90% when the average thickness is 2.1 layers (see Fig. 5). This verifies that the growth of consecutive layers over the first layer does not remain localized around the activation centres but
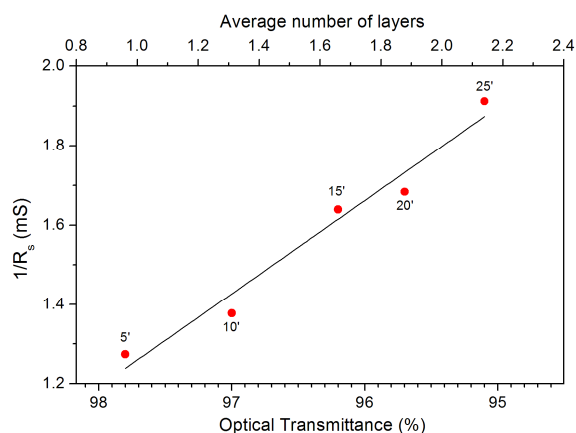
**Fig. 5** Conductivity of the CVD grown graphene films versus T, optical transmittance at 550nm and the average number of graphene layers, n. Labels by the data points mark the growth time; the line represents the linear fit with 0.534 mS/n.

uniformly extends over the whole surface.

The measured transmittance values of the graphene films at $\lambda$=550 nm vary between 95.1% and 97.8%. The optical transmittance data have been used to evaluate the average thickness of graphene by assuming 2.29% absorption per one layer of graphene.[62] The scatter plot in Fig. 5 displays the measured conductance ($\sigma = 1/R_s$) of the graphene films versus their optical transmittance, T as well as the calculated number of layers, n. In this graph, it is seen that $\sigma$ increases linearly with the average graphene thickness. This relation reveals uniform parallel conductance over multiple layers. The thickest grown film in the set of samples has the optical transmittance of 95.1% and the sheet resistance of $R_s = 520 \ \Omega/$ . Although the sheet resistance of the graphene films is still not as low as that of ITO[63], it can meet the $R_s$ and T requirements for some applications such as touch screens and flat panel displays.[30]

This non self-limiting multilayer growth, which has linear dependency of average thickness to the time, is not similar with earlier reports and cannot be explained with their proposed self-limited multilayer growth mechanism.[9,24,38–44] We believe it arises from the pressure level applied in this work that stands as an intermediate level compared to the low pressure ($\leq 1$ mbar), or atmospheric pressure (1000 mbar) growth methods commonly utilized in CVD applications. The intermediate pressure regime provides a straightforward control of the graphene thickness via adjustment of a single parameter, the growth time of the CVD process. This pressure level created a distinctive growth regime compared to both the low pressure CVD[38,48] and the atmospheric pressure CVD growth of graphene[38,49,50] and made it possible to control the film thickness and coverage only by tuning the growth time.

We argue that the scale of molecular mean free path, $\ell_{\text{mfp}}$ in comparison to the mean distance between the nucleation centers (while act as secondary carbon sources as well), $d$, plays a significant role in governing the growth regime (Fig. 6). The mean free path of gas particles can be deduced from the classical gas theory as $\ell_{mfp}=k_BT/(2^{1/2}\pi d_0^2 P)$, where $k_B$ is the Boltzmann constant, $T$ is the temperature, $P$ is pressure. Here $d_0$ is the diameter of the gas particles and its value is taken as 0.3 nm for this case. Another important length scale is represented by the thickness of the boundary layer, i.e. the active reaction zone where the process gas is stagnant above the surface. The boundary layer thickness in a laminar gas flow is given as $\delta \sim (\mu/nv)^{1/2}$, where $\mu$, $v$ and $n$ are the viscosity, velocity and the density of the gas respectively. Although exact value of $\delta$ depends on geometry and location as well its variation with P is relatively small since it scales as $\delta \sim 1/P^{1/2}$ while $\ell_{mfp} \sim 1/P$. While $\ell_{\text{mfp}} \approx 0.3$ µm at the atmospheric pressure, it extends to about 5 µm when the process pressure is set to 60 mbar as implemented in this work. For this range of pressure, $\delta$ changes only by a factor of 4. During the multilayer growth process, the active carbon species are generated at the impurity sites and they diffuse away until either bonding to a graphene edge site and contribute to the multilayer growth or they leave the boundary layer site and carried away. Therefore, $\ell_{mfp}$ plays a central role in governing the size of the graphene islands. At around atmospheric pressure level the growth is limited to microscopic sizes, but for P~60 mbar the active carbon species are able to move several microns from their sources within the boundary layer. This provides a condition for the growth of relatively large single crystal graphene islands. When the mean distance between the
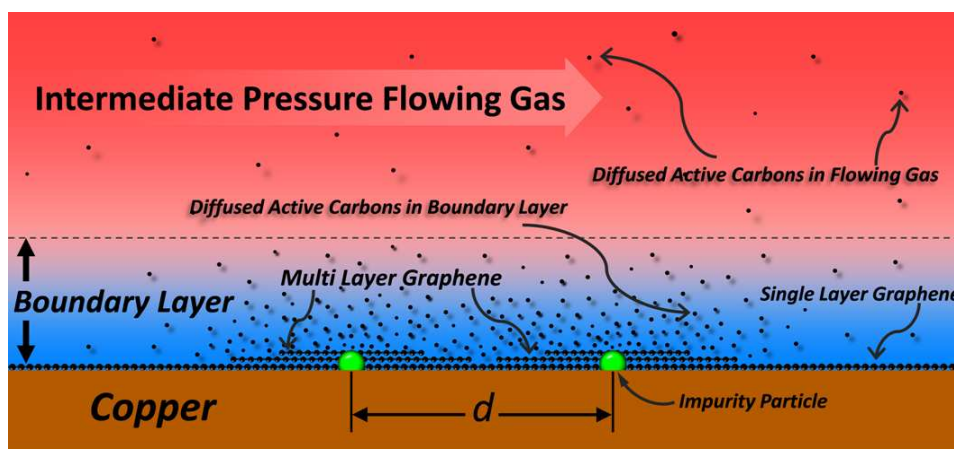


**Fig. 6** Schematic representation of the proposed impurity mediated growth kinetics of multilayer graphene on copper surface. Although the first layer is formed by surface adsorption, the consecutive layers are seeded by the impurities. The size of the multiple layer graphene is determined by the relative scales of the molecular mean free path, $\ell_{\text{mfp}}$ and the mean distance between the carbon sources, d. Intermediate pressure (this work), $\ell_{\text{mfp}}$~ d; growth of ML graphene islands seeded by impurities extend and results in full coverage of ML over the surface.

# ARTICLE TYPE

nucleation sites, $d$ is in the same length scale as the size of the graphene islands, full coverage of multilayer graphene over the surface is accomplished. Here the role of impurity particles is central for multilayer growth; they act both as the catalysts[55–58]
5 and the nucleation sites for multilayer graphene islands. For the experiments presented in this work, these particles that are distributed over the surface with mean separation $d = 6$ μm in between them (close to $\ell_{mfp}$ value) permits the full coverage of multilayer graphene through the merger of initially isolated
10 islands.

In the case of low pressure CVD, the graphene growth on copper is mainly governed by surface adsorption and is self-limited to single layer. Since $\ell_{mfp}$ becomes much larger than $\delta$, the active carbon species emerging from these point sources can
15 rapidly leave out the boundary layer, diffuse in main flowing gas stream and will be carried away before they can adhere to a site on the surface to form multiple layer graphene (Fig. 6). Therefore, in the low pressure CVD, there is not much contribution from the impurities and multilayer growth does not
20 occur. In case of atmospheric pressure CVD, the growth is facilitated by the limited diffusion through the boundary layer. Therefore, multilayer graphene islands form around the surface impurities and defects; however their range is reduced due to short molecular mean free path $\ell_{mfp}$, within the gas. These two
25 extreme pressure regimes have been analysed through a kinetic model and observed in a number of experiments.[38,48–50]

Directly testing the effect of pressure could strengthen our understanding along this model. However, it should be noted that controlling pressure independent of other process parameters
30 such as flow rates and gas concentrations is experimentally challenging.

## Conclusions

We performed controllable CVD growth of multilayer graphene by controlling growth time, under fixed intermediate pressure and
35 fixed temperature. Optical microscopy, scanning electron microscopy, Raman analysis and electrical conductivity measurements consistently show the uniform expansion of multilayer islands with growth time. Although graphene growth on copper at low pressure is known to be mediated by surface
40 adsorption, we claim that the multilayer growth can be boosted in presence of impurities and a tuned process pressure. It seems when the pressure is adjusted to an intermediate level such that the mean free path and average distance between the activation sites are comparable, the formation of multilayer graphene
45 islands can be enhanced to achieve full surface coverage. Under such conditions, the multilayer coverage and average graphene thickness increase as the growth time is increased in a wide range of 5 to 25 minutes, verifying the non-localized nature of the multilayer growth. We believe that this work can contribute to
50 understanding of the kinetics of CVD growth of multilayer

graphene on copper surface.

## Notes and references

[a]Faculty of Engineering and Natural Sciences, Sabanci University,
55 34956 Istanbul, Turkey.
[b]Nanotechnology Research and Application Center, Sabanci University,
34956 Istanbul, Turkey.
E-mail:iikaya@sabanciuniv.edu; Tel: +90 216 4839591

60 1  A. H. Castro Neto, F. Guinea, N. M. R. Peres, K. S. Novoselov and a. K. Geim, *Rev. Mod. Phys.*, 2009, **81**, 109–162.
2  K. I. Bolotin, K. J. Sikes, Z. Jiang, M. Klima, G. Fudenberg, J. Hone, P. Kim and H. L. Stormer, *Solid State Commun.*, 2008, **146**, 351–355.
65 3  Y. Zhang, T.-T. Tang, C. Girit, Z. Hao, M. C. Martin, A. Zettl, M. F. Crommie, Y. R. Shen and F. Wang, *Nature*, 2009, **459**, 820–823.
4  Z. C. Gomez De Arco L, Zhang Y, Schlenker CW, Ryu K, Thompson ME, *ACS Nano*, 2010, **4**, 2865–73.
5  X. Miao, S. Tongay, M. K. Petterson, K. Berke, A. G. Rinzler, B. R.
70  Appleton and A. F. Hebard, *Nano Lett.*, 2012, **12**, 6–11.
6  B. J. Kim, H. Jang, S. K. Lee, B. H. Hong, J. H. Ahn and J. H. Cho, *Nano Lett.*, 2010, **10**, 3464–3466.
7  Y. Wang, Z. Shi, Y. Huang, Y. Ma, C. Wang, M. Chen and Y. Chen, *J. Phys. Chem. C*, 2009, **113**, 13103–13107.
75 8  S. Paek, E. Yoo and I. Honma, *Nano Lett.*, 2009, **9**, 72–75.
9  Ö. B. Ni GX, Zheng Y, Bae S, Tan CY, Kahya O, Wu J, Hong BH, Yao K, *ACS Nano*, 2012, **6**, 3935–3942.
10  P. Blake, P. D. Brimicombe, R. R. Nair, T. J. Booth, D. Jiang, F. Schedin, L. a. Ponomarenko, S. V. Morozov, H. F. Gleeson, E. W.
80  Hill, A. K. Geim and K. S. Novoselov, *Nano Lett.*, 2008, **8**, 1704–1708.
11  J. D. Fowler, M. J. Allen, V. C. Tung, Y. Yang, R. B. Kaner and B. H. Weiller, *ACS Nano*, 2009, **3**, 301–306.
12  K. S. Novoselov, D. Jiang, F. Schedin, T. J. Booth, V. V Khotkevich,
85  S. V Morozov and a K. Geim, *Proc. Natl. Acad. Sci. U. S. A.*, 2005, **102**, 10451–10453.
13  S. Stankovich, D. a. Dikin, R. D. Piner, K. a. Kohlhaas, A. Kleinhammes, Y. Jia, Y. Wu, S. T. Nguyen and R. S. Ruoff, *Carbon N. Y.*, 2007, **45**, 1558–1565.
90 14  C. Berger, Z. Song, T. Li, X. Li, A. Y. Ogbazghi, R. Feng, Z. Dai, A. N. Marchenkov, E. H. Conrad, P. N. First and W. a de Heer, *J.Pyhs.Chem.B*, 2004, **108**, 19912–19916.
15  X. Li, W. Cai, J. An, S. Kim, J. Nah, D. Yang, R. Piner, A. Velamakanni, I. Jung, E. Tutuc, S. K. Banerjee, L. Colombo and R.
95  S. Ruoff, *Science*, 2009, **324**, 1312–1314.
16  S. Bae, H. Kim, Y. Lee, X. Xu, J.-S. Park, Y. Zheng, J. Balakrishnan, T. Lei, H. R. Kim, Y. Il Song, Y.-J. Kim, K. S. Kim, B. Ozyilmaz, J.-H. Ahn, B. H. Hong and S. Iijima, *Nat. Nanotechnol.*, 2010, **5**, 574–578.
100 17  K. S. Kim, Y. Zhao, H. Jang, S. Y. Lee, J. M. Kim, K. S. Kim, J.-H. Ahn, P. Kim, J.-Y. Choi and B. H. Hong, *Nature*, 2009, **457**, 706–710.
18  A. Reina, S. Thiele, X. Jia, S. Bhaviripudi, M. S. Dresselhaus, J. a. Schaefer and J. Kong, *Nano Res.*, 2009, **2**, 509–516.
105 19  B. J. Kang, J. H. Mun, C. Y. Hwang and B. J. Cho, *J. Appl. Phys.*, 2009, **106**.
20  L. Gao, W. Ren, J. Zhao, L. P. Ma, Z. Chen and H. M. Cheng, *Appl. Phys. Lett.*, 2010, **97**.
21  R. John, a Ashokreddy, C. Vijayan and T. Pradeep, *Nanotechnology*,
110  2011, **22**, 165701.

22  B. Wang, Y. Zhang, Z. Chen, Y. Wu, Z. Jin, X. Liu, L. Hu and G. Yu, *Mater. Lett.*, 2013, **93**, 165–168.

23  C.-M. Seah, S.-P. Chai and A. R. Mohamed, *Carbon N. Y.*, 2014, **70**, 1–21.

24  S. M. Kim, A. Hsu, Y.-H. Lee, M. Dresselhaus, T. Palacios, K. K. Kim and J. Kong, *Nanotechnology*, 2013, **24**, 365602.

25  G. H. Han, F. Güneş, J. J. Bae, E. S. Kim, S. J. Chae, H. J. Shin, J. Y. Choi, D. Pribat and Y. H. Lee, *Nano Lett.*, 2011, **11**, 4144–4148.

26  A. E. Al Reina and A. et al Reina, *Nano Lett.*, 2009, **9**, 30–35.

27  S. Bae, S. J. Kim, D. Shin, J.-H. Ahn and B. H. Hong, *Phys. Scr.*, 2012, **T146**, 014024.

28  S. Pang, Y. Hernandez, X. Feng and K. Müllen, *Adv. Mater.*, 2011, **23**, 2779–2795.

29  T. Sun, Z. L. Wang, Z. J. Shi, G. Z. Ran, W. J. Xu, Z. Y. Wang, Y. Z. Li, L. Dai and G. G. Qin, *Appl. Phys. Lett.*, 2010, **96**, 10–13.

30  J. Wu, M. Agrawal, A. Becerril, Z. Bao, Z. Liu, Ḱ. Y. Chen and P. Peumans, *ACS Nano*, 2010, **4**, 43–48.

31  Y. Zhang, L. Zhang and C. Zhou, *Acc. Chem. Res.*, 2013, **46**, 2329–2339.

32  M. Singh, H. S. Jha and P. Agarwal, *Mater. Lett.*, 2014, **126**, 249–252.

33  Y. H. Zhang, Z. Y. Chen, B. Wang, Y. W. Wu, Z. Jin, X. Y. Liu and G. H. Yu, *Mater. Lett.*, 2013, **96**, 149–151.

34  N. Kishi, A. Fukaya, R. Sugita, T. Kado, T. Soga and T. Jimbo, *Mater. Lett.*, 2012, **79**, 21–24.

35  C. Mattevi, H. Kim and M. Chhowalla, *J. Mater. Chem.*, 2011, **21**, 3324.

36  J. W. Wood, Joshua D., Schmucker, Scott W., Lyons, Austin S., Pop, Eric, Lyding, *Nano Lett.*, 2011, **11**, 4547–4554.

37  X. Li, W. Cai, L. Colombo and R. S. Ruoff, *Nano Lett.*, 2009, **9**, 4268–4272.

38  S. Bhaviripudi, X. Jia, M. S. Dresselhaus and J. Kong, *Nano Lett.*, 2010, **10**, 4128–4133.

39  K. Yan, H. Peng, Y. Zhou, H. Li and Z. Liu, *Nano Lett.*, 2011, **11**, 1106–1110.

40  Z. Tu, Z. Liu, Y. Li, F. Yang, L. Zhang, Z. Zhao, C. Xu, S. Wu, H. Liu, H. Yang and P. Richard, *Carbon N. Y.*, 2014, **73**, 252–258.

41  Z. Yan, Y. Liu, L. Ju, Z. Peng, J. Lin, G. Wang, H. Zhou, C. Xiang, E. L. G. Samuel, C. Kittrell, V. I. Artyukhov, F. Wang, B. I. Yakobson and J. M. Tour, *Angew. Chemie - Int. Ed.*, 2014, **53**, 1565–1569.

42  W. Fang, A. L. Hsu, R. Caudillo, Y. Song, a. G. Birdwell, E. Zakar, M. Kalbac, M. Dubey, T. Palacios, M. S. Dresselhaus, P. T. Araujo and J. Kong, *Nano Lett.*, 2013, **13**, 1541–1548.

43  Q. Li, H. Chou, J. H. Zhong, J. Y. Liu, A. Dolocan, J. Zhang, Y. Zhou, R. S. Ruoff, S. Chen and W. Cai, *Nano Lett.*, 2013, **13**, 486–490.

44  M. Kalbac, O. Frank and L. Kavan, *Carbon N. Y.*, 2012, **50**, 3682–3687.

45  Z. Luo, T. Yu, J. Shang, Y. Wang, S. Lim, L. Liu, G. G. Gurzadyan, Z. Shen and J. Lin, *Adv. Funct. Mater.*, 2011, **21**, 911–917.

46  O. Frank, J. Vejpravova, V. Holy, L. Kavan and M. Kalbac, *Carbon N. Y.*, 2014, **68**, 440–451.

47  I. Vlassiouk, P. Fulvio, H. Meyer, N. Lavrik, S. Dai, P. Datskos and S. Smirnov, *Carbon N. Y.*, 2013, **54**, 58–67.

48  M. Regmi, M. F. Chisholm and G. Eres, *Carbon N. Y.*, 2012, **50**, 134–141.

49  V. T. Nguyen, H. D. Le, V. C. Nguyen, T. T. Tam Ngo, D. Q. Le, X. N. Nguyen and N. M. Phan, *Adv. Nat. Sci. Nanosci. Nanotechnol.*, 2013, **4**, 035012.

50  M. P. Lavin-Lopez, J. L. Valverde, M. C. Cuevas, a Garrido, L. Sanchez-Silva, P. Martinez and a Romero-Izquierdo, *Phys. Chem. Chem. Phys.*, 2014, **16**, 2962–70.

51  L. Huang, Q. H. Chang, G. L. Guo, Y. Liu, Y. Q. Xie, T. Wang, B. Ling and H. F. Yang, *Carbon N. Y.*, 2012, **50**, 551–556.

52  H. J. Park, J. Meyer, S. Roth and V. Skákalová, *Carbon N. Y.*, 2010, **48**, 1088–1094.

53  S. Chen, W. Cai, R. D. Piner, J. W. Suk, Y. Wu, Y. Ren, J. Kang and R. S. Ruoff, *Nano Lett.*, 2011, **11**, 3519–3525.

54  a. Delamoreanu, C. Rabot, C. Vallee and a. Zenasni, *Carbon N. Y.*, 2014, **66**, 48–56.

55  H. Yang, L. Huang, Q. H. Chang, Z. J. Ma, S. H. Xu, Q. Chen and W. Z. Shi, *J. Phys. D. Appl. Phys.*, 2014, **315101**.

56  D. Yu, Q. Zhang and L. Dai, *J.AM.CHEM.SOC.*, 2010, **132**, 15127–15129.

57  Z. Liu, Y.-C. Lin, C.-C. Lu, C.-H. Yeh, P.-W. Chiu, S. Iijima and K. Suenaga, *Nat. Commun.*, 2014, **5**, 4055.

58  A. Bachmatiuk, F. Börrnert, M. Grobosch, F. Schäffel and U. Wolff, *ACS Nano*, 2009, **3**, 3–5.

59  D. Graf, F. Molitor, K. Ensslin, C. Stampfer, a. Jungen, C. Hierold and L. Wirtz, *Nano Lett.*, 2007, **7**, 238–242.

60  Y. ~Y. Wang and Et Al., *J. Phys. Chem. C*, 2008, **112**, 10637–10640.

61  A. C. Ferrari, J. C. Meyer, V. Scardaci, C. Casiraghi, M. Lazzeri, F. Mauri, S. Piscanec, D. Jiang, K. S. Novoselov, S. Roth and a. K. Geim, *Phys. Rev. Lett.*, 2006, **97**, 1–4.

62  R. R. Nair, P. Blake, a N. Grigorenko, K. S. Novoselov, T. J. Booth, T. Stauber, N. M. R. Peres and a K. Geim, *Science*, 2008, **320**, 1308.

63  J. Y. Lee, S. T. Connor, Y. Cui and P. Peumans, *Nano Lett.*, 2008, **8**, 689–692.